

Relationship between the ideality factor and the iron concentration in silicon solar cells

O.Ya. Olikh

Faculty of Physics, Taras Shevchenko National University of Kyiv, Kyiv 01601, Ukraine

Abstract

The ideality factor value of silicon $n^+ - p$ solar cells with a various iron contaminant has been studied by means of computer simulation. An iron concentration range of $10^{10} - 10^{13} \text{ cm}^{-3}$, a base doping level range of $10^{15} - 10^{17} \text{ cm}^{-3}$, and a temperature range of $290 - 340 \text{ K}$ were under study. The Solar Cells Capacitance Simulator (SCAPS) has been the tool used for numerical simulation of these devices. The two-diode model was used to extract an ideality factor. The Shockley–Read–Hall recombination, the Auger recombination, the radiative recombination, the unpaired interstitial iron, and the iron–boron pair were under consideration. The algorithms of an iron concentration evaluation in a silicon solar cell by using a current–voltage curve have been proposed. The analytic expressions have been suggested and the calibration curves have been calculated.

Keywords: silicon solar cell, SCAPS simulator, ideality factor, iron concentration

1. Introduction

It is well known that impurities are crucial for the semiconductor devices performance. It is completely relevant to solar cell (SC) as well. Dopants determinate an internal electric field, which leads to a separation of light-generated carriers and a photovoltage generation. Contaminants act often as a highly effective recombination centre, reducing the carrier lifetime and SC efficiency. Therefore the impurity concentration determination is a very important problem. There are many experimental methods for solving this problem, such as the infrared spectroscopy, deep level transient spectroscopy, photoluminescence, thermally stimulated capacitance and current, secondary ion mass spectrometry etc [1]. These methods are complicated enough and demand a special setup.

At the same time, the analysis of the current–voltage ($I - V$) characteristic is commonly used to characterize the solar cell. Thus, the dark $I - V$ curve normally serves as a first diagnosis of SC recombination [2]. The $I - V$

Email address: olikh@univ.kiev.ua (O.Ya. Olikh)

equation that models the SC by an equivalent electrical circuit contains several parameters related to physical phenomena occurring in the device. It is obviously that these parameters depend on impurities, but the interrelations are intricate sufficiently. As a result, $I - V$ curves are not used practically for a contaminant diagnosis, although the possibility of simultaneous calibrate both SC performance and impurity looks quite attractive.

One of a number of parameters of SC model is the ideality factor n . The value of $n > 1$ indicates that there are traps involved in a carrier recombination mechanism in solar cells. If the defect related recombination is dominant than the value $n = 2$ is often stated in a literature. But when the value of n approaches 2, it suggests the very specific assumptions about the energy levels (middle of the bandgap) and capture cross sections (equal for electrons and holes) of the recombination centres in a symmetrically doped diode which lead to $n = 2$ [3, 4]. Typically, the value of the ideality factor ranges from 1 to 2 for real devices and depends on ambient conditions and the recombination center parameters, including a trap concentration [4–8]. Thus, the ideality factor is an important parameter that can describe the electrical behavior of photovoltaic devices and is used to characterize the recombination in SC [9].

The aim of our work is to investigate a possibility of a contaminant concentration evaluation by using an ideality factor value. The heuristic approach is used and its milestones can be expressed as following: i) the dark $I - V$ characteristic of the SCs with known contaminant composition is simulated; ii) the obtained characteristic is fitted according to the double-diode model and the ideality factor is determined; iii) the initial impurity concentration and the calculated ideality factor value are used for acquisition of analytic or grading dependencies.

As a first approximation, the paper considers a fairly simple but practically important system. Namely, the crystalline silicon SC and iron impurity were under consideration. Si photovoltaic device cover almost 90% of global SC market. Iron is a major contaminant due to the wide use of stainless steel equipment in the fabrication line and one of the most detrimental metal impurities in solar-grade crystalline silicon materials [10–12].

Numerical simulation is carried out by using the one-dimensional code SCAPS [13, 14]. This software is widely used to modeling of various solar cells [15–21], including silicon based devices [19–21].

2. Simulation details

2.1. Solar cell structure and material parameters

The simple $n^+ - p$ structure as shown in inset in Fig. 2 is used in the present calculation. with the initial thickness of each layer $d_n = 0.5 \mu\text{m}$ and $d_p = 300 \mu\text{m}$, respectively. n^+ is the emitter layer with $N_D = 10^{19} \text{ cm}^{-3}$ while $10^{15} - 10^{17} \text{ cm}^{-3}$ is the N_A of the p base layer. The p base layer is uniformly doped with boron.

The simulations were carried out over a temperature range of 290 \div 330 K. The temperature dependencies of bandgap and carrier mobility are calculated,

respectively, according to Varshni and Caughey–Thomas equations [1]. The bandgap narrowing is considered as described by the Slotboom equation [22, 23]. The density of states in the conduction/valence band (N_C/N_V) and thermal carrier velocities are from Green [24].

The iron is considered as a base layer uniform contaminant with the concentration $10^{10}–10^{13} \text{ cm}^{-3}$. The iron atoms are known to be predominantly located in interstitial lattice position in silicon. The donor level $E_{\text{Fe}_i} = E_V + 0.394 \text{ eV}$ is associated with Fe_i [25, 26]. Therefore neutral Fe_i^0 and ionized Fe_i^+ interstitial are observed in Si. In *p*-type material, Fe_i^+ readily interacts with ionized shallow acceptors. In our simulation, the pair Fe_iB_s must be under consideration. On the one hand, this pair is bistable defect and the trigonal and the orthorhombic configurations are feasible. On the other hand, the orthorhombic pair is only observable at low temperature ($< 150 \text{ K}$) under an illumination or carrier injection condition [27, 28]. Besides, the Fe_iB_s pairs can be readily dissociated by 15 to 90 s illumination with a halogen lamp [11]. The association reaction is diffusion limited and can take place under dark condition during tens minute [29]. Two following cases were under simulation.

i) The negligible proportion of Fe present in the form of Fe_iB_s pairs is assumed:

$$N_{\text{Fe}} = N_{\text{Fe}_i^0} + N_{\text{Fe}_i^+}, \quad (1)$$

where $N_{\text{Fe}_i^0}$ and $N_{\text{Fe}_i^+}$ are the concentrations of neutral and ionized iron respectively. This is a safe assumption for cells operating under constant illumination or after illumination stop immediately. The hole and electron capture cross-sections of defect are calculated according to $\sigma_{p,\text{Fe}_i} = 3.85 \times 10^{-16} \exp(-\frac{0.045}{kT}) \text{ cm}^2$ and $\sigma_{n,\text{Fe}_i} = 9.1 \times 10^{-15} \exp(-\frac{0.024}{kT}) \text{ cm}^2$ [10, 25, 26]. E_{Fe_i} is taken as the temperature independent value [30]. This case is labeled “FI” from now on.

ii) The equilibrium condition is assumed and the total dissolved iron concentration is given by a sum of concentrations of three separate species

$$N_{\text{Fe}} = N_{\text{Fe}_i^0} + N_{\text{Fe}_i^+} + N_{\text{FeB}}, \quad (2)$$

where N_{FeB} is the Fe_iB_s pair concentration. The using of the relationships between the equilibrium concentration of Fe_i^+ , Fe_i^0 , and Fe_iB_s from [26, 29] leads to the following expression

$$N_{\text{FeB}} = N_{\text{Fe}} \frac{N_A 10^{-23} \exp\left(-\frac{E_b}{kT}\right)}{\left[1 + N_A 10^{-23} \exp\left(-\frac{E_b}{kT}\right)\right] \left[1 + \exp\left(-\frac{F - E_{\text{Fe}_i}}{kT}\right)\right]}. \quad (3)$$

where F is the Fermi level, E_b is the binding energy of the Fe_iB_s pairs (taken as 0.582 eV). Hence it should be taken under account the uniform distribution of the Fe_iB_s pair. In our simulation, first, the Fermi level position in the base layer is calculated for each doping level as well as temperature. Then, Eq. (3) is used to calculate the Fe_iB_s pair distribution. The representative example of calculation is shown in Fig. 1.

The trigonal Fe_iB_s pair is considered, a true condition under room temperature. This pair is amphoteric defect. In the present work, the parameters of

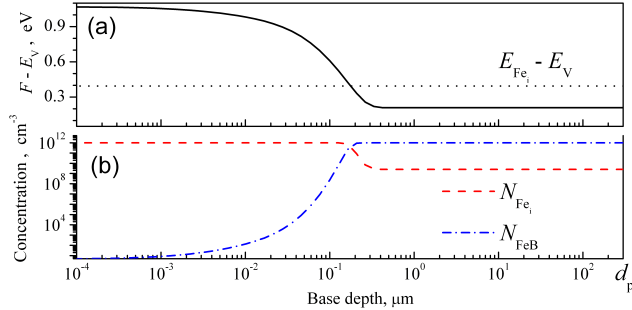


Figure 1: The calculated SC base distribution of Fermi level position (a, solid line), unpaired interstitial iron concentration (b, dashed line), and Fe_iB_s pair concentration (b, dotted-dashed line). $N_A = 10^{16} \text{ cm}^{-3}$, $T = 300 \text{ K}$. The position of Fe_i donor level (dotted line) is shown in the panel (a) as well.

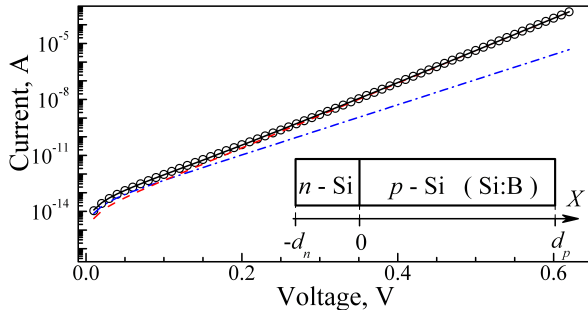


Figure 2: $I-V$ characteristic simulated in FI-SRH-case, $N_A = 10^{17} \text{ cm}^{-3}$, $N_{\text{Fe}} = 10^{13} \text{ cm}^{-3}$, $T = 290 \text{ K}$ (marks) and its fitting by Eq. (4) (solid line). The dashed and dotted-dashed lines represent the diffusion and recombination currents. Inset: Solar cell structure, which are used in simulation.

donor ($E_{\text{FeB}}^d = E_V + 0.10 \text{ eV}$, $\sigma_{p,\text{FeB}}^d = 2 \times 10^{-14} \text{ cm}^2$, $\sigma_{n,\text{FeB}}^d = 4 \times 10^{-13} \text{ cm}^2$) and acceptor ($E_{\text{FeB}}^a = E_C - 0.26 \text{ eV}$, $\sigma_{p,\text{FeB}}^a = 5.5 \times 10^{-15} \text{ cm}^2$, $\sigma_{n,\text{FeB}}^a = 2.5 \times 10^{-15} \text{ cm}^2$) levels are used from [10, 25, 26, 29]. This case is labeled ‘‘FIFB’’ from now on.

Only a bulk recombination is under consideration in the paper. Once again two cases were simulated. In the first one, labeled ‘‘SRH’’, the Shockley–Read–Hall recombination is taken into account only. In the second one, denoted ‘‘SRHBBA’’, the both Shockley–Read–Hall recombination and intrinsic recombination are allowed for. The electron and hole Auger recombination factors ($C_n = 2.8 \times 10^{-31} \text{ cm}^6 \text{s}^{-1}$ and $C_p = 9.9 \times 10^{-32} \text{ cm}^6 \text{s}^{-1}$) and radiative band-to-band recombination coefficient ($B = 1.8 \times 10^{-15} \text{ cm}^3 \text{s}^{-1}$) are taken from [22].

So, four different data sets (FI-SRH, FI-SRHBBA, FIFB-SRH, and FIFB-SRHBBA) have been simulated for solar cell.

The dark forward $I - V$ characteristic were generated by SCAPS over a

voltage range up to 0.62 V. The $I - V$ curve example is shown in Fig. 2.

The real silicon SCs are often described by so-called two-diode model [31]. The first diode represents the “ideal” diode, describing the so-called diffusion current, characterized by a saturation current I_{01} , and the second diode is the so-called recombination current, characterized by a saturation current I_{02} and an ideality factor n [31]. According to the two-diode model, the dark SC current is given by

$$I = I_{01} \left[\exp \left(-\frac{qV}{kT} \right) - 1 \right] + I_{02} \left[\exp \left(-\frac{qV}{nkT} \right) - 1 \right]. \quad (4)$$

It should be noted that the influence of series resistance as well as shunt resistance is neglected in Eq. (4). We used Eq. (4) to fit the simulated data taking n , I_{01} , and I_{02} as the fitting parameters and more attention was paid to the ideality factor value. The fitting result is shown in Fig. 2.

All non-linear fittings in the paper were done by using the differential evolution method [32, 33]. The least-squares method was used to linear fitting.

3. Results and Discussion

3.1. Interstitial iron, SRH recombination

Some data, calculated in the FI-SRH case, are shown in Fig. 3(a,b). One can see that the ideality factor increases monotonically with the doping level increase. While temperature dependence of the n is more intricate: it contains the both increasing and decreasing components and the contribution of the last one rises with increase in N_A . The iron concentration increase leads to the increase in n value and does not change $n(N_A, T)$ dependence — see Fig. 3 and Supplementary Material. It is evidence of for possibilities of N_{Fe} evaluation by using n . Only low doping level value ($N_A \cong 10^{15} \text{ cm}^{-3}$) and high temperature ($T > 300 \text{ K}$) are exclusion because $n \cong 1$ is expected accordingly to the simulation.

It is clear that an analytical expression would be more convenient way to the N_{Fe} evaluation. To build such expression one has to take into account that the interstitial iron captures an electron in p -type silicon. Therefore the recombination affectivity is determined by a hole occurrence on the Fe_i level.

The hole occupation probability is $f_p = \left[1 + \exp \left(\frac{F - E_{\text{Fe}_i}}{kT} \right) \right]^{-1}$ and this equation can be a start point to build an expression $n = n(T, N_A, N_{Fe})$. It must be considered that, unlike the simulated $n(N_A, T)$ relationship, $f_p(N_A, T)$ depends on temperature monotonically and reaches saturation with the increase in N_A — see Supplementary Material. In addition, the Fermi level can be evaluated by the equation $(F - E_V) = kT \ln(N_V/N_A)$ under the simulation conditions.

Based on aforesaid, we search expression $n = n(T, N_A, N_{Fe})$ in the following form:

$$n(T, N_A, N_{Fe}) = 1 + \frac{n_0(N_{Fe}) \cdot T^{m_T} \cdot (\log N_A)^{m_A}}{1 + N_V(T) \cdot \gamma(N_A, N_{Fe}) \cdot \exp \left(\frac{E_{\text{ef}}(T, N_A)}{kT} \right)}, \quad (5)$$

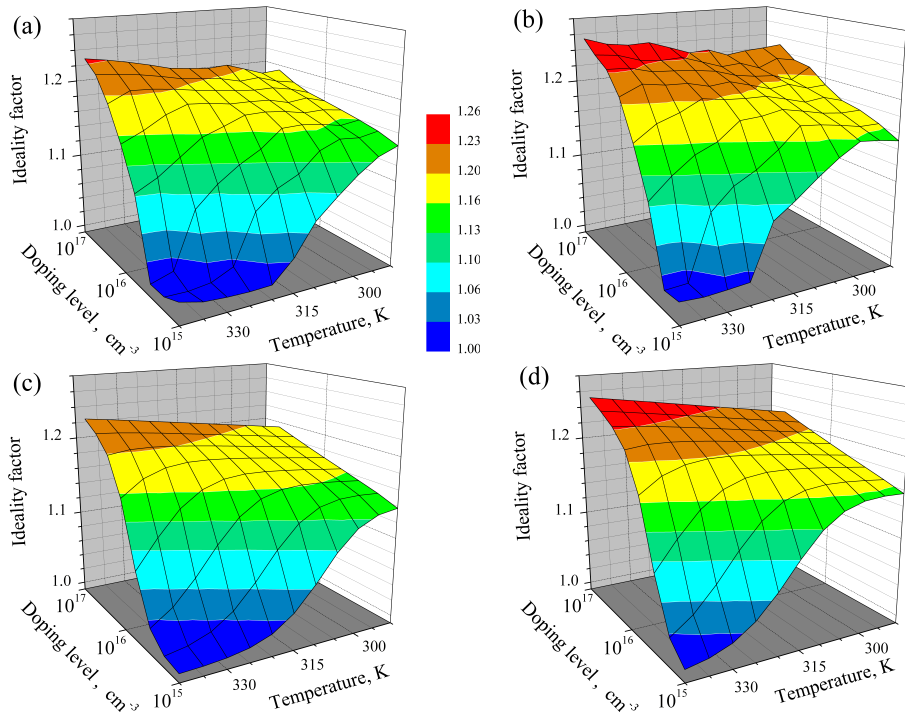


Figure 3: Ideality factor as a function of the temperature and dopant (boron) concentration. FI-SRH case. N_{Fe} , cm^{-3} : 10^{10} (a,c), 10^{13} (b,d). The simulated data are in panels (a) and (b); the fittings of simulated data with help Eq. (5) are in panels (c) and (d).

Table 1: Parameters of Eq. (5) fitting of simulated ideality factor relationships.

Simulation case	Parameter		
	m_T	m_A	γ (cm ³)
FI-SRH	1.13	2.85	N_A^{-1}
FI-SRHBBA	1.3	2.85	Eq. (9)
FIFB-SRH	2.2	2.85	Fig. 9(a)
FIFB-SRHBBA	2.2	2.85	Fig. 9(b)

where m_T and m_A are the constant, and fitness parameters n_0 , γ , and E_{ef} depend on iron concentration, doping level, and temperature.

The analysis has shown that the simulated data are well fitted by Eq. (5) with $m_T = 1.13$, $m_A = 2.85$, $\gamma = N_A^{-1}$. Besides, the dependence of the effective energy E_{ef} can be expressed as:

$$E_{\text{ef}}(T, N_A) = E_0 - \alpha T / \log N_A + \beta T, \quad (6)$$

where values $E_0 = 1.43 \pm 0.08$ eV, $\alpha = 85 \pm 5$ meV cm⁻³K⁻¹, and $\beta = 1.9 \pm 0.2$ meV K⁻¹ do not depend on N_{Fe} practically. The parameters are listed in Table 1 and the results of the fitting are shown in Fig. 3(c,d), and Supplementary Material. A good agreement of simulated data and fitting curves prove the expediency of Eq. (5) using.

Thus, in the FI-SRH case, the simulated (semi-empirical) dependence of the ideality factor takes the following shape:

$$n = 1 + \frac{n_0(N_{\text{Fe}}) \cdot T^{1.13} \cdot (\log N_A)^{2.85}}{1 + \frac{N_V(T)}{N_A} \cdot \exp\left(\frac{1.43}{kT} - \frac{986}{\log N_A} + 22\right)}. \quad (7)$$

We use Eq. (7) by taking n_0 as fitting parameter to fit the n dependencies, calculated for different N_{Fe} value. The resulting n_0 dependence on iron concentration is shown in Fig. 4. This curve is monotonic as well as smooth enough and can serve as a calibration curve. In addition, the found dependence is well described by Eq. (8):

$$n_0(N_{\text{Fe}}) = 1.28 \times 10^{-7} - \frac{2.38 \times 10^{-8}}{1 + \left(\frac{N_{\text{Fe}}}{4.96 \times 10^{12}}\right)^{0.85}}. \quad (8)$$

Thus, the algorithm of an iron concentration evaluation in a silicon SC by using a $I - V$ curve can be as following.

- (i) The solar cell is illuminated by 15 to 90 s with a halogen lamp to dissociate the FeB pairs. When illumination stopped, the $I - V$ characteristic is measured.
- (ii) $I - V$ curve is fitted accordingly to the two-diode model and the ideality factor n is determined.

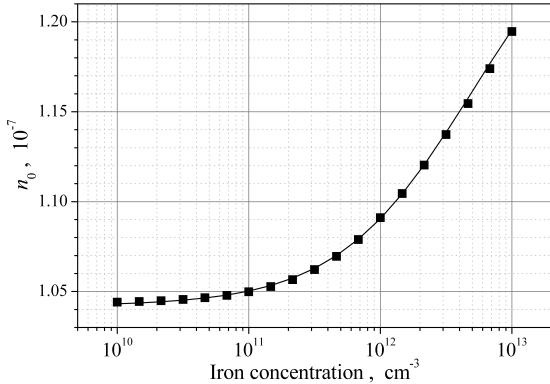


Figure 4: Dependence of the parameter n_0 (see Eq. (5)) on the iron concentration in SC base. FI-SRH case. Line is the fitted curve using Eq. (8).

- (iii) Taking into account n value, doping level N_A , and measurement temperature, the parameter n_0 is calculated by relationship

$$n_0 = (n - 1) \cdot \frac{1 + \frac{N_V(T)}{N_A} \cdot \exp\left(\frac{1.43}{kT} - \frac{986}{\log N_A} + 22\right)}{T^{1.13} \cdot (\log N_A)^{2.85}}.$$

- (iv) N_{Fe} is evaluated by using the calibration curve in Fig. 4 or by the following expression

$$N_{Fe} = 4.96 \times 10^{12} \cdot \left(\frac{2.38 \times 10^{-8}}{1.28 \times 10^{-7} - n_0} \right)^{1.18}.$$

3.2. Interstitial iron, SRH recombination, intrinsic recombination

It should be noted that the taking into consideration of the Auger recombination and band-to-band recombination cause to modification in the above algorithm. In fact, the simulation show that the dependencies $n(N_A, T)$ are changed partially — see Fig. 5. It is quite expectable that these changes rise with the N_A increase and the N_{Fe} decrease. Besides, the non-monotonic dependencies $n(N_A, T)$ are observed at the low iron concentration value. Thus, the search for an analytical expression, qualified for the each temperature and doping level values, seems inappropriate.

On the other hand, since room temperature measurements of $I - V$ characteristics alone cannot provide detailed information about the SC properties, additional insight is often gained by characterising the devices over a temperature range. Therefore in this case, we try to evaluate the iron concentration by using the ideality factor temperature dependence, which is measured (simulated) for the solar cell with the known constant doping level — $n(T) |_{N_A=\text{const}}$.

Some of the obtained curves $n(T)$ are shown in Fig. 6. One can see that the N_A value affects substantively on temperature dependence of the ideality

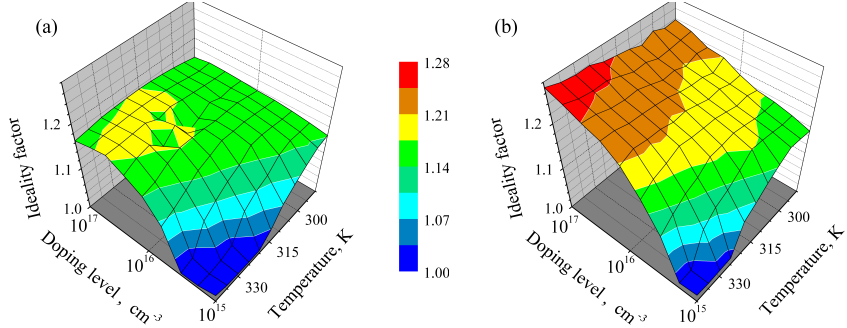


Figure 5: Ideality factor as a function of the temperature and dopant (boron) concentration. FI-SRHBBA case. N_{Fe} , cm^{-3} : 10^{10} (a), 10^{13} (b).

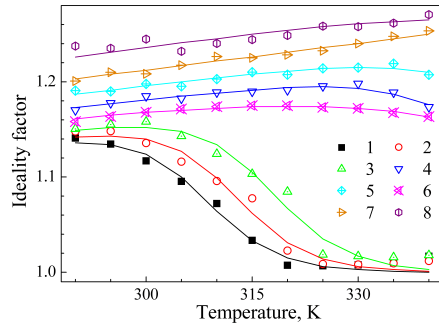


Figure 6: Temperature dependencies of the ideality factor. FI-SRHBBA case. The marks are the simulation results, and the lines are the fitted curves using Eq. (5) and data in Table 1. N_{Fe} , cm^{-3} : 10^{10} (curves 1, 6), 10^{12} (2, 4, and 7), 10^{13} (3, 5, and 8). N_A cm^{-3} : 10^{15} (1, 2, and 3), 10^{16} (4, 5), 10^{17} (6, 7, and 8).

factor. We use Eq. (5) and value $m_A = 2.85$ to fit the simulated n temperature dependence. A close agreement between simulated and fitted data has been found with help $m_T = 1.3$ and $E_{\text{ef}} = (9.53 - 0.52 \log N_A)$ — see lines in Fig. 6.

The values of the both another parameters n_0 and γ depend on doping level as well as iron concentration and can be used to evaluate N_{Fe} . So, as it is shown in Fig. 7(a), the dependencies $\gamma(N_{\text{Fe}})$ can be described by the following equation:

$$\gamma = \left(\frac{10^{15}}{N_A} \right)^{11} \cdot \frac{\eta N_0 + N_{\text{Fe}}}{N_0 + N_{\text{Fe}}} . \quad (9)$$

where $10 \div 15$ and $(0.5 \div 1) \times 10^{12} \text{ cm}^{-3}$ are the η and N_0 , respectively, at various boron concentration.

The concentration dependencies of the parameter n_0 are shown in Fig. 7(b) and can serve as a calibration curves as well. As shown in figure, the iron concentration evaluation by using the n_0 value is advisable for a high base doping level ($N_A > 10^{16} \text{ cm}^{-3}$). At low N_A value the weak dependence n_0

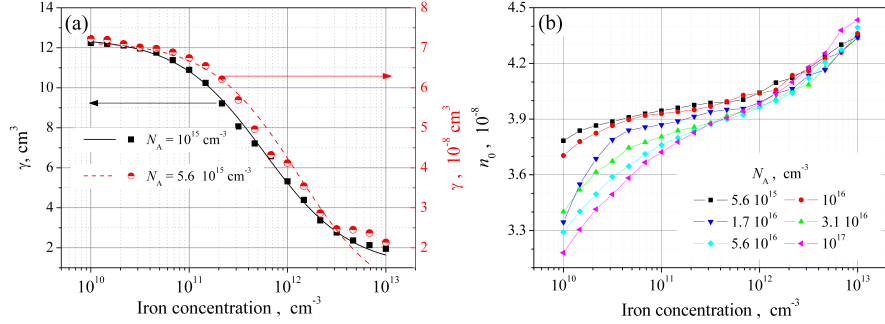


Figure 7: Dependencies of the parameters γ (a) and n_0 (b) on the iron concentration in SC base. FI-SRHBBA case. Lines in panel (a) are the fitted curves using Eq. (9), lines in panel (b) only serve as guide to the eye.

on N_{Fe} impairs the estimation accuracy. Simultaneously, the opposite case is observed for parameter γ and it is better to evaluate N_{Fe} by the γ value at a low doping level. Otherwise the γ decreases significantly (see Eq. (9)) and the accuracy of γ determination by Eq. (5) fitting falls.

3.3. Iron–boron pair and interstitial iron

The results, obtained under an equilibrium condition and Fe_iB_s presence, are illustrated by Fig. 8. The main features of the ideality factor change are obviously to be in agree with the case of Fe_iB_s absent. Namely, there are n increase with increase in N_{Fe} , the $n(T)$ dependence non-monotony, which pronounced with decrease in N_A , etc. First of all, these are because Fermi level is far from the valence band, the neutral interstitial Fe_i^0 is dominant, and the boron contained complex is not created within a space charge region (SCR) — see Fig. 1. That is, unlike the quasi neutral region, the illumination does not cardinally change the N_{Fe_i} and $N_{\text{Fe}_i\text{B}_s}$ ratio. On the other hand, the SCR recombination defines the value of ideality factor mainly. But the n absolute value is smaller in FIFB-case than that in the FI-case because Fe_i and Fe_iB_s have different energy levels and cross-sections for recombination. Comparison of Fig. 8(a) and Fig. 8(c) as well as comparison of Fig. 8(b) and Fig. 8(d) shows that intrinsic recombination affects the n value at a low iron concentration, and high temperature, and high doping level.

As in previous FI-SRHBBA case, the different $n(N_A, T)$ dependencies are observed at the different N_{Fe} values. As in previous case, the ideality factor temperature dependencies $n(T) |_{N_A=\text{const}}$ are under consideration and we use Eq. (5) to fit simulated data. It has been found that the simulated data are in good agreement with the fitting curves (see Supplementary Material) for values $m_T = 2.2$ and E_{ef} , which were linear dependent of $\log N_A$ and were listed in Table 1.

The obtained dependencies of parameters γ and n_0 on iron concentration are shown in Fig. 9 and Fig. 10, respectively, and can serve as a calibration

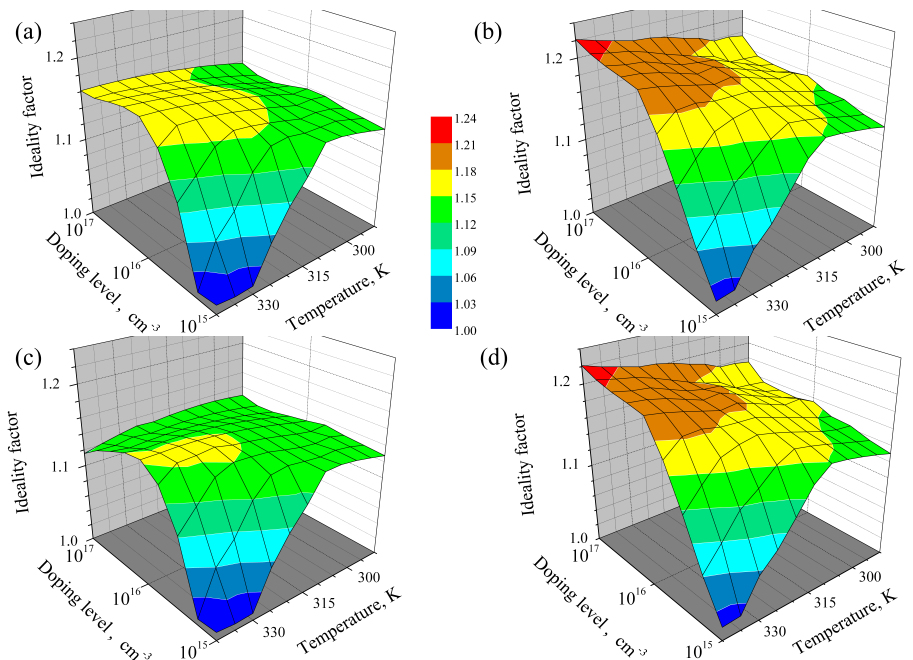


Figure 8: Ideality factor as a function of the temperature and dopant (boron) concentration. FIFB-SRH (a,b) and FIFB-SRHBBA (c, d) cases. N_{Fe} , cm^{-3} : 10^{10} (a, c), 10^{13} (b, d).

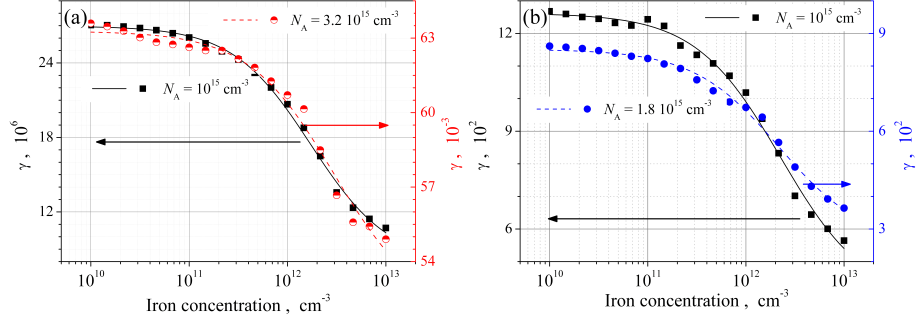


Figure 9: Dependencies of the parameters γ on the iron concentration in SC base. FIFB–SRH (a) and FIFB–SRHBBA (b) cases. Lines are the fitted curves using Eq. (9)

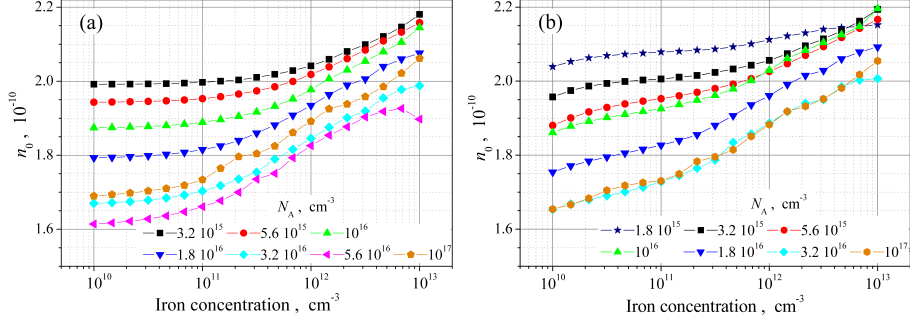


Figure 10: Dependencies of the parameters n_0 on the iron concentration in SC base. FIFB–SRH (a) and FIFB–SRHBBA (b) cases. Lines only serve as guide to the eye.

curves as well. Again, it is more appropriate to use the parameter γ for N_{Fe} evaluation at low boron concentrations and the parameter n_0 in the opposite case. However, the conditional limit shifts toward the smaller N_A values and is about $3 \times 10^{15} \text{ cm}^{-3}$. Again, the main difference between calibration curves in the FIFB–SRH and FIFB–SRHBBA cases is observed for $N_A < 10^{11} \text{ cm}^{-3}$ and $N_A > 3 \times 10^{16} \text{ cm}^{-3}$.

Thus, the another, more complicated but more general, algorithm of an iron concentration evaluation can be offered.

- (i) The dark $I - V$ characteristics of the silicon SC are measured over over a temperature range of about 290 – 340 K. The measurements can be carried out after a halogen lamp illumination or after long-term storing in the dark.
- (ii) $I - V$ curves are fitted accordingly to the two-diode model and the temperature dependency of the ideality factor $n(T)$ is determined.
- (iii) Eq. (5) and Table 1 are used to fit the $n(T)$. The n_0 and γ are taken as the fitting parameters.
- (iv) N_{Fe} is evaluated by using calibration curves in Fig. 7 or in Figs. 9(b) and

10(b) in the after illumination or after dark storing measurement cases, respectively.

4. Conclusion

The relationship between the diode ideality factor and the iron concentration in the base layer of silicon $n^+ - p$ solar cells has been studied through computer simulation. An iron concentration range of $10^{10} - 10^{13} \text{ cm}^{-3}$, a base doping level range of $10^{15} - 10^{17} \text{ cm}^{-3}$, and a temperature range of $290 - 340 \text{ K}$ were under study. The results obtained in this work show that the ideality factor value can serve to estimate a contaminant concentration. So, the analysis has shown that in the case of the Shockley–Read–Hall recombination and the unpaired interstitial iron, single $I - V$ characteristic measurement and single ideality factor extraction are needed. If the Auger recombination, the radiative recombination, or the iron–boron pair presence have to be taking into account, then measurements over a temperature range are needed. The calibration curves have been calculated and the analytic expressions have been suggested.

However we should note the following. The simplified task was under consideration and the set of variables consisted of three values (temperature, doping level, iron concentration) only. But the analytical expression was found in the approximation case only. As simulation has shown, the geometry of the solar cell (e.g. base layer thickness) affected value of ideality factor as well. In general case, the ideality factor can be used to estimate not only a trap concentration but also an energy level and a capture cross-section. But such multivariable problem would lead to a huge set of calibration curves. On the other hand, the artificial neural networks seem to be good for this task.

References

References

- [1] D. K. Schroder, Semiconductor Material and Device Characterization, 3rd Edition, John Wiley & Sons, New Jersey, 2006.
- [2] S. Grover, A. J. V. Li, D. L. Young, P. Stradins, H. M. Branz, Reformulation of solar cell physics to facilitate experimental separation of recombination pathways, *Appl. Phys. Lett.* 103 (9) (2013) 093502. doi:10.1063/1.4819728.
- [3] R. Kuhn, P. Fath, E. Bucher, Effects of pn-junctions bordering on surfaces investigated by means of 2D-modeling, in: Conference Record of the Twenty-Eighth IEEE Photovoltaic Specialists Conference – 2000 (Cat. No.00CH37036), 2000, pp. 116–119. doi:10.1109/PVSC.2000.915768.
- [4] J. Beier, B. Voss, Humps in dark I–V–curves–analysis and explanation, in: Conference Record of the Twenty Third IEEE Photovoltaic Specialists Conference - 1993 (Cat. No.93CH3283-9), 1993, pp. 321–326. doi:10.1109/PVSC.1993.347163.

- [5] K. McIntosh, P. Altermatt, G. Heiser, Depletion–region recombination in silicon solar cells. when does $mdr = 2$?, in: 16th European Photovoltaic Solar Energy Conference: Proceedings of the International Conference and Exhibition, Publisher:James and James (Science Publishers) Ltd, 2000, pp. 250–253.
- [6] A. Kaminski, J. J. Marchand, H. El Omari, A. Laugier, Q. N. Le, D. Sarti, Conduction processes in silicon solar cells, in: Conference Record of the Twenty Fifth IEEE Photovoltaic Specialists Conference – 1996, 1996, pp. 573–576. doi:10.1109/PVSC.1996.564071.
- [7] Z. Hameiri, K. McIntosh, G. Xu, Evaluation of recombination processes using the local ideality factor of carrier lifetime measurements, Sol. Energy Mater. Sol. Cells 117 (2013) 251–258. doi:10.1016/j.solmat.2013.05.040.
- [8] A. S. H. van der Heide, A. Schonecker, J. H. Bultman, W. C. Sinke, Explanation of high solar cell diode factors by nonuniform contact resistance, Progress in Photovoltaics: Research and Applications 13 (1) (2005) 3–16. doi:10.1002/pip.556.
- [9] L. Duan, H. Yi, C. Xu, M. B. Upama, M. A. Mahmud, D. Wang, F. H. Shabab, A. Uddin, Relationship between the diode ideality factor and the carrier recombination resistance in organic solar cells, IEEE Journal of Photovoltaics 8 (6) (2018) 1701–1709. doi:10.1109/JPHOTOV.2018.2870722.
- [10] A. A. Istratov, H. Hieslmair, E. Weber, Iron and its complexes in silicon, Applied Physics A: Materials Science & Processing 69 (1) (1999) 13–44. doi:10.1007/s003390050968.
- [11] J. Schmidt, Effect of dissociation of iron–boron pairs in crystalline silicon on solar cell properties, Progress in Photovoltaics: Research and Applications 13 (4) (2005) 325–331. doi:10.1002/pip.594.
- [12] H. Zhu, X. Yu, X. Zhu, Y. Wu, J. He, J. Vanhellemont, D. Yang, Low temperature iron gettering by grown-in defects in p–type Czochralski silicon, Superlattices Microstruct. 99 (2016) 192–196. doi:10.1016/j.spmi.2016.03.006.
- [13] M. Burgelman, P. Nollet, S. Degrave, Modelling polycrystalline semiconductor solar cells, Thin Solid Films 361–362 (2000) 527–532. doi:10.1016/S0040-6090(99)00825-1.
- [14] K. Decock, S. Khelifi, M. Burgelman, Modelling multivalent defects in thin film solar cells, Thin Solid Films 519 (21) (2011) 7481–7484. doi:10.1016/j.tsf.2010.12.039.
- [15] M. Cappelletti, G. Casas, A. Cdola, E. P. y Blanc, B. M. Soucase, Study of the reverse saturation current and series resistance of p-p-n perovskite solar cells using the single and double-diode models, Superlattices Microstruct. 123 (2018) 338–348. doi:10.1016/j.spmi.2018.09.023.

- [16] M. Mostefaoui, H. Mazari, S. Khelifi, A. Bouraiou, R. Dabou, Simulation of high efficiency CIGS solar cells with SCAPS-1D software, *Energy Procedia* 74 (2015) 736–744. doi:10.1016/j.egypro.2015.07.809.
- [17] C.-H. Huang, W.-J. Chuang, Dependence of performance parameters of CdTe solar cells on semiconductor properties studied by using SCAPS-1D, *Vacuum* 118 (2015) 32–37. doi:10.1016/j.vacuum.2015.03.008.
- [18] F. Azri, A. Meftah, N. Sengouga, A. Meftah, Electron and hole transport layers optimization by numerical simulation of a perovskite solar cell, *Solar Energy* 181 (2019) 372–378. doi:10.1016/j.solener.2019.02.017.
- [19] A. Hamache, N. Sengouga, A. Meftah, M. Henini, Modeling the effect of 1 MeV electron irradiation on the performance of n⁺-p-p⁺ silicon space solar cells, *Radiat. Phys. Chem.* 123 (2016) 103–108. doi:10.1016/j.radphyschem.2016.02.025.
- [20] E. Hu, G. Yue, R. Zhang, Y. Zheng, L. Chen, S. Wang, Numerical simulations of multilevel impurity photovoltaic effect in the sulfur doped crystalline silicon, *Renewable Energy* 77 (2015) 442–446. doi:10.1016/j.renene.2014.12.049.
- [21] B. Zhao, J. Zhou, Y. Chen, Numerical simulation of the impurity photovoltaic effect in silicon solar cells doped with thallium, *Physica B: Condensed Matter* 405 (18) (2010) 3834–3837. doi:10.1016/j.physb.2010.06.012.
- [22] A. McEvoy, T. Markvart, L. Castaner (Eds.), *Solar Cells. Materials, Manufacture and Operation*, 2nd Edition, Academic Press, Oxford, 2013.
- [23] Z. Zhou, I. Perez-Wurfl, B. J. Simonds, Rapid, deep dopant diffusion in crystalline silicon by laser-induced surface melting, *Mater. Sci. Semicond. Process.* 86 (2018) 8–17. doi:10.1016/j.mssp.2018.06.012.
- [24] M. A. Green, Intrinsic concentration, effective densities of states, and effective mass in silicon, *J. Appl. Phys.* 67 (6) (1990) 2944–2954. doi:10.1063/1.345414.
- [25] S. Rein, S. W. Glunz, Electronic properties of interstitial iron and iron-boron pairs determined by means of advanced lifetime spectroscopy, *J. Appl. Phys.* 98 (11) (2005) 113711. doi:10.1063/1.2106017.
- [26] J. D. Murphy, K. Bothe, M. Olmo, V. V. Voronkov, R. J. Falster, The effect of oxide precipitates on minority carrier lifetime in p-type silicon, *J. Appl. Phys.* 110 (5) (2011) 053713. doi:10.1063/1.3632067.
- [27] T. Nærland, S. Bernardini, N. Stoddard, E. Good, A. Augusto, M. Bertoni, Comparison of iron-related recombination centers in boron, gallium, and indium doped silicon analyzed by defect parameter contour mapping, *Energy Procedia* 124 (2017) 138–145. doi:10.1016/j.egypro.2017.09.321.

- [28] S. Sakauchi, M. Suezawa, K. Sumino, H. Nakashima, Recombination-enhanced Fe atom jump between the first and the second neighbor site of Fe–acceptor pair in Si, *J. Appl. Phys.* 80 (11) (1996) 6198–6203. doi:10.1063/1.363695.
- [29] W. Wijaranakula, The reaction kinetics of iron–boron pair formation and dissociation in p-type silicon, *J. Electrochem. Soc.* 140 (1) (1993) 275–281. doi:10.1149/1.2056102.
- [30] H. Kohno, H. Hieslmair, A. A. Istratov, E. R. Weber, Temperature dependence of the iron donor level in silicon at device processing temperatures, *Appl. Phys. Lett.* 76 (19) (2000) 2734–2736. doi:10.1063/1.126459.
- [31] O. Breitenstein, Understanding the current-voltage characteristics of industrial crystalline silicon solar cells by considering inhomogeneous current distributions, *Opto-Electronics Review* 21 (3) (2013) 259–282. doi:10.2478/s11772-013-0095-5.
- [32] J. Sun, Q. Zhang, E. P. Tsang, DE/EDA: A new evolutionary algorithm for global optimization, *Inform. Sci.* 169 (3–4) (2005) 249–262. doi:10.1016/j.ins.2004.06.009.
- [33] K. Wang, M. Ye, Parameter determination of Schottky–barrier diode model using differential evolution, *Solid-State Electron.* 53 (2) (2009) 234–240. doi:10.1016/j.sse.2008.11.010.